

# **Practical Implementation of a Concept for In-Situ Detection of Humidity-Related Degradation of IGBT Modules**

Benedikt Kostka, Axel Mertens  
Institute for Drive Systems and Power Electronics  
Welfengarten 1A  
30167 Hanover, Germany  
Phone: +49 (0) 511-762 18833  
Email: Benedikt.Kostka@ial.uni-hannover.de  
URL: <https://www.ial.uni-hannover.de>

July 14, 2022

## **Acknowledgments**

This work is part of the project ReCoWind and was funded by the Federal Ministry for Economic Affairs and Climate Action on the basis of a decision by the German Bundestag. Funding number: 0324336E. The authors are responsible for the content of this publication.

Special thanks go to CONVERTERTEC GMBH for providing the back-to-back converter investigated.

## **Keywords**

«Breakdown», «Condition monitoring», «IGBT», «Power semiconductor device», «Reliability».

## **Abstract**

The high voltage, high humidity, high temperature, reverse bias (HV-H<sup>3</sup>TRB) test reveals that humidity affects the blocking characteristic of an IGBT module, resulting in increased leakage current, decreased voltage blocking capability, or some combination of these. This paper presents the practical implementation of a previously proposed measurement concept for in-situ detection of moisture-induced degradation of IGBT modules in a full-scale back-to-back converter for doubly fed electrical machines typically used in wind turbines.

## **Introduction**

In recent years, various field data analyses have found a correlation between relative ambient humidity and the failure rate of wind turbines [1], [2]. It has been shown that the phase module, which consists of the semiconductor modules and the DC-link capacitor, is responsible for a large proportion of the failures. Furthermore, the failures are more likely to occur during the start-up process after the wind turbines have been subjected to a prolonged standstill period [2]. Indeed, [3] shows that IGBT modules can be damaged by moisture by exposing the devices to the HV-H<sup>3</sup>TRB test. Consequences can include reduced voltage-blocking capability and increased leakage current.

Therefore, further investigations into the condition monitoring of the system, especially the power semiconductors, are necessary. There are a lot of publications covering the online determination of the junction temperature of an IGBT using temperature-sensitive parameters (TSEPs) and/or online detection of temperature-related degradation, such as bond wire liftoff and solder joint fatigue [4], [5]. However, to date, there have been only a few publications that deal with online condition monitoring with regard

to moisture-related degradation or moisture in the inverter itself, with the aim of estimating its electrochemical condition on the basis of service life models (e.g., Peck's Model) [6]. A first approach for monitoring humidity-related degradation of semiconductors is presented in [7]; a concept is detailed that enables the in-situ measurement of a device state inside an inverter by measuring the blocking characteristics of IGBTs in a half-bridge configuration. However, the results have only been obtained on a laboratory scale. Based on the findings in [7], this paper presents the practical implementation of the concept in a full-scale, back-to-back converter typically used for doubly fed electrical machines in wind turbines.

The structure of the paper is as follows. First, the functional principle of the concept under investigation is explained and a functional description of the hardware developed is given. Then the implementation of the measurement board in the converter is described. Next, the measurements, which are initially carried out with non-degraded modules, are presented. Afterwards, the measurements are also conducted with previously degraded modules connected to the inverter under test. Finally, a conclusion to this work is given.

## Measurement Concept

In this section, the developed measurement concept is presented. After the general function is explained, the structure of the developed hardware is described.

## Principle of Operation

The general idea of the condition-monitoring concept is shown in Fig. 1 (left). The concept is designed to conduct the measurement during the standstill phases of the wind turbine, as restarting the wind turbine after downtime increases the risk of a phase module failure [8]. In this state, the switches (e.g., IGBT modules) are actively switched off and a DC-link voltage  $V_{dc}$  must be applied. To detect module degradation before it becomes critical, the DC link must be precharged above its nominal voltage  $V_{dc,N}$ . Ideally, the DC-link voltage should be at least as high as the highest voltage occurring during normal operation (e.g., the overvoltage during IGBT switch-off). This can be realised, for example, by using a precharging transformer, which is usually used in wind turbines and must be adapted for a higher voltage. The load machine connected to the phase terminals acts like a DC short circuit between all phases during the measurement.

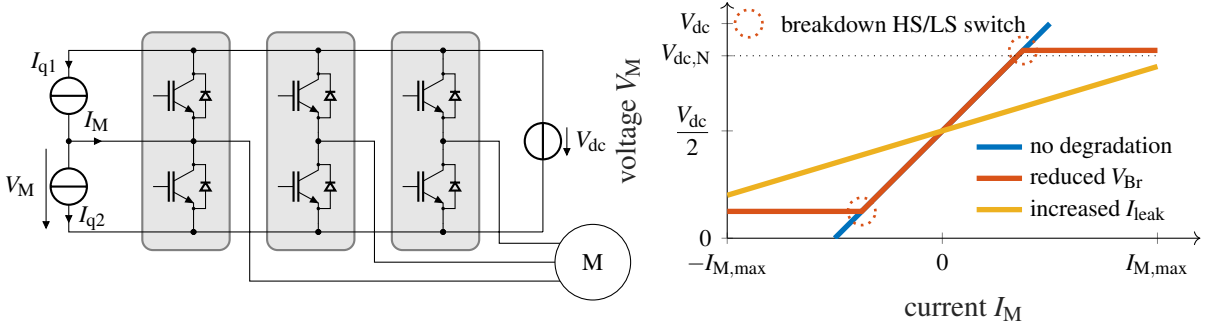


Fig. 1: Measurement concept for detecting moisture-related damage to semiconductor chips in a three-phase inverter (left); Possible  $I_M$ - $V_M$  waveforms for the same states of degradation of the high-side and low-side switches (right)

The concept is based on two additional DC current sources ( $I_{q1}$  and  $I_{q2}$ ). These inject a measuring current  $I_M$  into the phase terminals which corresponds to the difference between  $I_{q1}$  and  $I_{q2}$ . Since the voltage  $V_M$  depends on the leakage currents of the switched-off high-side and low-side switches, the voltage  $V_M$  is adjusted using the current  $I_M$ . Safe operation of the concept is ensured so long as the combined breakdown voltage of the high-side and low-side switches is greater than the applied DC-link voltage  $V_{dc}$ .

The voltage across the low-side switches ( $V_{LS} = V_M$ ) increases with increasing positive current  $I_M$ . It continues to rise until either the applied DC-link voltage  $V_{dc}$  is reached, a premature avalanche of the low-side switches is detected, or the leakage current of the low-side switches at  $V_{dc}$  is higher than the positive maximum current of  $I_M$ , which is limited by the additional current sources. As would be expected, the voltage  $V_M$  decreases when the current  $I_M$  decreases, because then the voltage across the high-side switches increases and the voltage across the low-side switches decreases ( $V_{HS} = V_{dc} - V_M$ ). The voltage  $V_M$  will decrease until it reaches 0 V, a premature avalanche of the high-side switches is detected, or the leakage current of the high-side switches at  $V_{dc}$  is higher than the negative maximum current of  $I_M$ , which is limited by the additional current sources. The maximum current limits  $I_{M,max}$  and  $-I_{M,max}$  must be chosen carefully so that detection of degradation is possible, but also so that the current does not destroy the semiconductor components in the inverter.

Fig. 1 (right) outlines three possible  $I_M$ - $V_M$  characteristics, which assume that the state of degradation of the high-side and low-side switches is the same. Thus, for a given voltage, the same leakage current flows through both the high-side and low-side switches, and all  $I_M$ - $V_M$  characteristics cross at the point  $V_M = \frac{V_{dc}}{2}$  and  $I_M = 0$  A.

The blue line shows the case in which no degradation of the modules is observed. In this case, the voltage  $V_M$  increases with increasing current  $I_M$ . Consequently, as the current decreases, the voltage also decreases. As  $V_M$  reaches the value of the applied DC-link voltage  $V_{dc}$  or 0 V, it can be stated that the high-side and low-side switches have a blocking capability of at least  $V_{dc}$ . A more detailed characterisation is not possible at this point.

In contrast, the red line shows the case in which the maximum breakdown voltage of the high-side and low-side switches is reduced, such as might result from degradation caused by humidity. Since only a reduction in breakdown voltage and no increase in leakage current is assumed, the red line coincides with the blue line in the area where no breakdown is provoked. As soon as the voltage  $V_M$  reaches the breakdown voltage of the low-side switches, the current  $I_M$  immediately increases to the maximum current value  $I_{M,max}$  without any significant change in the voltage  $V_M$ . Here, the exact value of the breakdown voltage of the weakest low-side switch can be determined directly from the measurement data. The procedure is similar for the high-side switches, except that now the voltage  $V_M$  decreases as the current  $I_M$  decreases. This means that the voltage across the high-side switches increases. Thus, as the voltage  $V_M$  decreases further, the breakdown of the weakest high-side switch is triggered and the current  $I_M$  falls to its maximum negative value  $-I_{M,max}$  without the voltage  $V_M$  changing significantly.

The yellow line shows the  $I_M$ - $V_M$  characteristic for an increased leakage current through the high-side and low-side switches without a drop in breakdown voltage. As can be seen in Fig. 1 (right), an increase in the leakage current through the modules from DC+ to DC- reduces the influence of the injected current  $I_M$  on the voltage  $V_M$ . If the leakage current through the low-side switches at  $V_{dc}$  is greater than  $I_{M,max}$ , then  $V_M$  does not reach the applied DC-link voltage  $V_{dc}$ . The same applies to the high-side switches, with the difference that  $V_M$  does not then reach 0 V. The voltage value  $V_M$  at maximum negative current and maximum positive current is therefore an indicator of whether or not degradation of the blocking characteristics has occurred, which could be caused by humidity.

## Hardware

Fig. 2 (left) shows the printed circuit board (PCB) designed for this concept. The PCB has the size of 130 mm x 70 mm with a voltage rating of 1400 V. Furthermore, Fig. 2 (right) shows the schematic and the main components used on the PCB.

In general, only two additional current sources need to be implemented, and these are attached to the DC link from DC+ to DC-. To inject the current  $I_M$ , the current sources  $I_{q1}$  and  $I_{q2}$  have to be connected to one of the phase terminals. Given the low power consumption of the concept, it can be fed directly from the power supply of the digital control unit (DCU) of the inverter and the injected current  $I_M$  is provided by the DC-link capacitor.

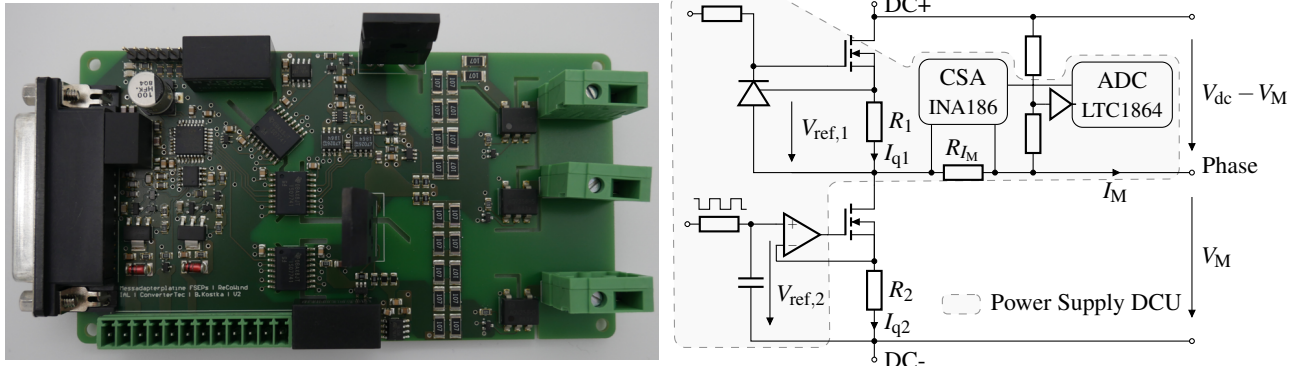


Fig. 2: Hardware design used in this work; Designed PCB (left); Simplified schematic (right)

$I_{q1}$  is implemented as a constant current source. It is built out of a high voltage blocking MOSFET, a resistor  $R_1$  and a shunt regulator. If the shunt regulator is fed with a sufficient current (approx. 200  $\mu$ A), it regulates the voltage  $V_{ref,1}$  occurring across the resistor  $R_1$  to a constant value. The MOSFET must be capable of blocking the whole applied DC-link voltage  $V_{dc}$ . The current  $I_{q1}$  can then be adjusted by choosing an appropriate value of  $R_1$ .

The principle of operation is similar for  $I_{q2}$ . But instead of a constant current, now an adjustable current is needed to adjust the current  $I_M$ , which is equal to the difference between  $I_{q1}$  and  $I_{q2}$  ( $I_M = I_{q1} - I_{q2}$ ). Therefore, no shunt regulator is used. Instead, the reference voltage  $V_{ref,2}$  is created by a PWM signal, which is filtered by a low-pass  $RC$  filter, so that  $V_{ref,2}$  corresponds to the product of the amplitude  $\hat{V}_{PWM}$  and the duty cycle  $d$  of the PWM signal ( $V_{ref,2} = d \cdot \hat{V}_{PWM}$ ). Since the subsequent operational amplifier (OPA) is installed with its inverting input directly connected to the source of the MOSFET and its output connected to the gate, the OPA regulates the output voltage so that the voltage at the inverting input corresponds to the voltage present at the non-inverting input  $V_{ref,2}$ . In this way, the current  $I_{q2}$  can be controlled by the duty cycle of the PWM signal provided by a microcontroller ( $\mu$ C).

To monitor the condition of the switches in the inverter, the current  $I_M$  and voltage  $V_M$  needs to be captured. The current measurement is performed with a shunt resistor in parallel to a current-sense amplifier (CSA). The current measurement range of the custom-designed PCB in Fig. 2 (left) is from  $I_{M,min} = -3.5$  mA to  $I_{M,max} = 5.8$  mA. The output voltage of the CSA is then recorded by an analog-to-digital converter (ADC). The recorded values are sent via the serial peripheral interface (SPI) to the  $\mu$ C, which sends the data to the processing unit (here: a computer) over a controller area network (CAN) bus. In contrast, the voltage  $V_M$  is captured with a high-impedance voltage divider. An identical ADC is used to record and send the measured data for  $V_M$  to the  $\mu$ C.

The measurement is started when the inverter is in an off state (i.e., a standstill phase of a wind turbine). All switches are then actively turned off and a DC-link voltage  $V_{dc}$ , which is higher than the nominal DC-link voltage  $V_{dc,N}$ , is applied. Afterwards, the PCB gets an signal to start the measurement. At the beginning, the duty cycle of the PWM signal is zero, which means that the reference voltage  $V_{ref,2}$  present at the resistor  $R_2$  is 0 V. So no current  $I_{q2}$  flows. In this case,  $I_M$  is equal to the constant current  $I_{q1}$ . In the following, the duty cycle is increased, which subsequently results in a reduction in the current  $I_M$  until the minimum current of  $I_M = I_{q1} - I_{q2,max}$  is reached.

## Experimental Implementation

The concept proposed in Fig. 1 (left) is implemented in a back-to-back converter typically used for doubly fed electrical machines in wind turbines. Fig. 3 shows the complete circuit diagram of the inverter including the additionally implemented measurement concept.

The converter consists of a line-side converter (LSC) connected to the grid via its three phases. The LSC converts the three-phase AC voltage into a DC voltage and feeds it into the DC link, which contains a

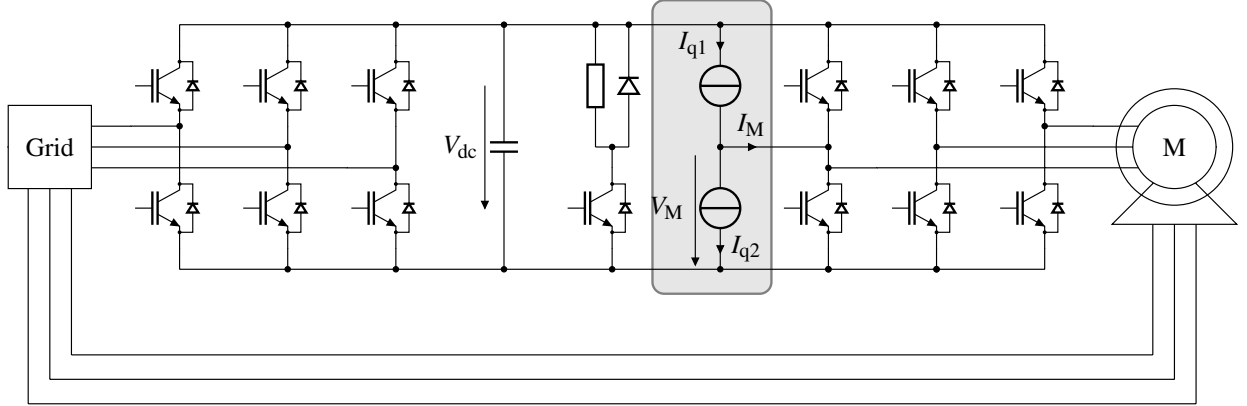


Fig. 3: Schematic of a back-to-back converter for doubly fed electrical machines with the integrated measurement concept at the machine-side converter

DC-link capacitor  $C_{dc}$  and a chopper. If the DC-link voltage exceeds a predefined value, the chopper switches on to limit the overvoltage and thus protect the components connected to the DC link. The resistor in series with the chopper switch is then connected directly to the DC link and dissipates the excess energy stored in  $C_{dc}$ . As a result, the DC-link voltage falls until the chopper switch is turned off again at a desired value of  $V_{dc}$ . As mentioned in [7], the chopper switch cannot be monitored using the proposed concept without further effort.

Therefore, the condition of the chopper switch needs to be investigated in advance in order to safely apply the proposed concept in a back-to-back converter for wind turbines. One option might be to measure the (very small) voltage drop across the chopper resistance to monitor the leakage current through the chopper. In this case, only an increase in the leakage current is detectable. Otherwise the chopper resistance must be disconnected, for example, by an additional contactor or relay. Then the condition of the chopper switch and diode might be monitored using the proposed concept in Fig. 1, in the same way as discussed in the previous section.

In addition to the LSC, a back-to-back converter also includes a machine-side converter (MSC) that shares the DC link with the LSC. The MSC converts the DC-link voltage into a three-phase AC voltage in order to drive the electrical machine. The three phases leaving the MSC are connected to the rotor of the electrical machine. In contrast, the stator of the doubly fed electrical machine is connected directly to the grid. Thus, power transfer between the grid and stator is also possible.

As shown in Fig. 3, the concept is integrated into the conventional back-to-back inverter. For the experiments conducted in this paper, the concept is connected to the second phase of the MSC. Furthermore, as mentioned in the previous section, the concept must be connected to the DC link. In the configuration shown in Fig. 3, only the condition of the switches in the MSC is monitored.

Since it is assumed that the wind turbine is in a standstill phase during the measurement, the converters (LSC and MSC) are actively switched off and are in a blocking state. Normally, no DC-link voltage is present at  $C_{dc}$  in this state. To carry out the measurement, the DC-link voltage  $V_{dc}$  must therefore be supplied externally. The applied DC-link voltage  $V_{dc}$  should be higher than the nominal DC-link voltage  $V_{dc,N}$ , but must be lower than the value at which the chopper switch is activated, otherwise the DC-link voltage would be discharged immediately. In the experiments conducted in this paper, the chopper switch was deactivated.

The DC-link capacitor  $C_{dc}$  can be precharged with the help of a precharge transformer, which wind turbines are often equipped with. In the converter investigated, the transformer is usually designed to precharge the DC link to a voltage of only 990 V, which is below the nominal DC-link voltage  $V_{dc,N}$  of the converter used. In this case, it is only possible to monitor modules that show an increase in leakage current as a result of humidity-related degradation. To detect a reduced blocking capability of the semiconductor components in the converter, the secondary voltage of the precharging transformer

must be adjusted, which is easily possible. The adjusted precharge transformer allows the precharging of the DC-link capacitor up to 1200 V. This means that the measurement concept may be applied to both converters (LSC and MSC) without any concerns regarding EMI, since no steep current or voltage slopes occur due to switching.

## Experimental Results

First, the designed measurement board in Fig. 2 (left) is mounted in a full scale back-to-back converter as shown in Fig. 3. Normally, the DC link can be precharged to a voltage of  $V_{dc} = 990$  V by the use of the precharge circuit. Since a higher DC-link voltage than the nominal DC-link voltage is needed to exploit the presented concept to its full extend, the precharge circuit is modified for the measurements presented in this paper. Now the DC link can be precharged to a voltage of  $V_{dc} = 1200$  V. The measured  $I_M$ - $V_M$  characteristics are recorded and plotted in Fig. 4 (left).

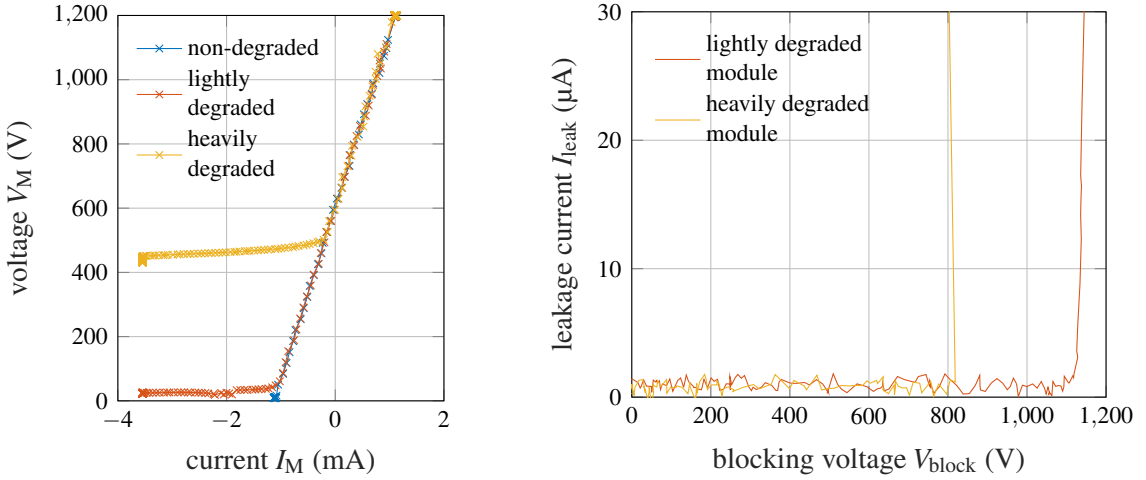


Fig. 4: Measured  $I_M$ - $V_M$  characteristic of the MSC when the DC link is precharged to a value of  $V_{dc} = 1200$  V using a modified precharge circuit (left); blocking characteristics of the modules previously degraded in the HV-H<sup>3</sup>TRB test (right)

During the measurements, the chopper is deactivated, since it would be triggered at a voltage of  $V_{dc} = 1170$  V and would discharge the DC-link capacitor immediately.

## Results without Degraded Modules

First of all, the measurement is carried out in the whole converter system without any emulation of humidity-related degradation. The  $I_M$ - $V_M$  characteristic obtained is shown in Fig. 4 (left) by the blue line. It reaches the maximum current of  $I_M \approx 1.1$  mA at a measured voltage of  $V_M$ , which is equal to the applied DC-link voltage of  $V_{dc} = 1200$  V. This means that the voltage across the high-side switches  $V_{HS}$  is equal to 0 V and the full DC-link voltage  $V_{dc}$  is applied across the low-side switches of the MSC ( $V_{LS} = V_{dc}$ ). Therefore, the measured current  $I_M$  here corresponds to the total leakage current through all the low-side switches connected in parallel, since the connected machine acts like a DC short between the three phases. However, the measured current of  $I_M \approx 1.1$  mA is quite high to be caused only by the semiconductors alone. The linear shape of the  $I_M$ - $V_M$  characteristic curve indicates resistive behaviour. This means that the characteristic of the intact modules is dominated by additional resistors and not by the semiconductors themselves. In the converter under investigation, the gate driver (GD) of the second phase has an additional measuring circuit for the collector-emitter voltage  $v_{ce}$ , which is provided with the help of a high-impedance voltage divider with a total resistance of  $1.62$  M $\Omega$ . Additionally, it should be noted that the GD of the first and third phases differs from the GD of the second phase, where the desaturation detection circuit is implemented using diodes. Therefore the leakage current of these GDs can be neglected in comparison to the leakage current of the GD of the second phase. Anyway, the measured equivalent resistance  $R_{M,LS}$  of the low side can easily be calculated as the ratio between the

applied DC-link voltage  $V_{dc}$  and the maximum of the measured current  $I_{M,max}$ , according to Ohm's law, since the voltage above the low side  $V_{LS}$  equals the measured voltage  $V_M$  ( $V_{LS} = V_M$ ).

$$R_{M,LS} = \frac{V_{dc}}{I_{M,max}} \quad . \quad (1)$$

Thus, this resistance is  $R_{M,LS} \approx 1.1 \text{ M}\Omega$ . In other words,  $R_{M,LS}$  is of the same order of magnitude as the resistance of the collector-sense circuit at the GD. As expected, the measured resistance is lower than the  $1.62 \text{ M}\Omega$  of the second phase's GD, since the other components (e.g. IGBT modules) connected from the phase to DC- contribute an additional leakage current which is also captured by the concept utilised. Since all phases can be considered parallel, the leakage current of all other components on the low side, except the  $1.62 \text{ M}\Omega$  resistance of the second phase's desaturation detection circuit, add up to  $360 \mu\text{A}$ . Obviously, the high leakage current is dominated by the resistance of the collector-sense circuit and not by the modules themselves.

Therefore, a very small change in leakage current cannot be detected with this setup. However, the datasheet states the maximum collector-emitter cut-off current to be as high as  $I_{CES} = 5 \text{ mA}$  at  $25^\circ\text{C}$  and the maximum applied collector-emitter voltage to be  $V_{ce} = 1700 \text{ V}$ . So it is possible to monitor a substantial increase in the leakage current of the modules in the range of  $\text{mA}$  as a sign of humidity-related degradation, even though this is still within the specification of the modules. This is sufficient for monitoring the condition of the modules.

Since the measured  $I_M-V_M$  characteristic is linear and reaches  $V_M = \frac{V_{dc}}{2} = 600 \text{ V}$  at  $I_M = 0 \text{ A}$ , it can be stated that the measured resistance of the high side is equal to the measured low-side resistance ( $R_{M,HS} = R_{M,LS}$ ). Otherwise  $R_{M,HS}$  can be calculated in the same way as  $R_{M,LS}$  in (1). The voltage above the high side  $V_{HS}$  is equal to the difference between the DC-link voltage  $V_{dc}$  and the measured voltage  $V_M$ .

$$V_{HS} = V_{dc} - V_M \quad . \quad (2)$$

According to (2), the whole DC-link voltage is applied to the high side when  $V_M$  is zero. Since no voltage is then applied to the low side, the whole (negative) current ( $-I_{M,max}$ ) is provided by the components of the high side at the applied DC-link voltage  $V_{dc}$ .

## Results with Degraded Modules

To emulate humidity-related degradation of an IGBT switch on the high side in the following, single-switch modules are connected in parallel to the high-side switches of the second phase of the MSC, which were previously degraded in the HV-H<sup>3</sup>TRB test. Fig. 4 (right) shows the blocking characteristics of the degraded modules. For more information about the test condition and underlying degradation mechanism, refer to [7]. In this work a lightly degraded module and a heavily degraded module are used. The lightly degraded module was kept for 168 hours under HV-H<sup>3</sup>TRB test conditions, while the heavily degraded module was kept for 1168 hours under the same conditions. As can be seen in Fig. 4 (right), both modules show a reduction in breakdown voltage but no increase in leakage current as signs of humidity-related degradation. For the lightly degraded module, the remaining maximum blocking voltage is approximately 1140 V and for the heavily degraded module it is approximately 800 V.

The obtained  $I_M-V_M$  characteristics for the MSC with the degraded modules connected to the high side of the second phase are shown in Fig. 4 (left). In the figure, the red line represents the measurement results with the lightly degraded module connected and the yellow line shows the results with the heavily degraded module connected. Both measured characteristics show a linear section which fits well to the measured  $I_M-V_M$  characteristic without any degraded module connected to the MSC. They both start at

the point  $V_M = V_{dc} = 1200\text{V}$  /  $I_M = 1.1\text{mA}$ . Obviously, no change to the low-side switches is detected, since no adjustments are done on the low side.

By reducing the current  $I_M$ , the voltage  $V_M$  decreases. Consequently, the voltage above the high side  $V_{HS}$  increases according to (2). For the red  $I_M$ - $V_M$  characteristic, the voltage  $V_M$  decreases linearly with the current  $I_M$  only until  $V_M$  is approximately 42 V. Then, the voltage  $V_M$  does not decrease significantly even though the current  $I_M$  is further reduced. This indicates that a breakdown on the high side is taking place. According to (2), the breakdown voltage of the high side for the  $I_M$ - $V_M$  characteristic with the lightly degraded module connected to the high side (see red line in Fig. 4 (left)) is determined to be approximately 1160 V. This fits well to the previously captured breakdown voltage of  $V_{BR} \approx 1140\text{V}$  of the lightly degraded module (red line in Fig. 4 (right)).

In contrast to this, for the yellow  $I_M$ - $V_M$  characteristic shown in Fig. 4 (left) when the heavily degraded module is connected to the high side, the breakdown is detected at a voltage of  $V_M = 490\text{V}$ . This corresponds to a determined breakdown voltage  $V_{BR} \approx 710\text{V}$  on the high side and is in good agreement with the captured blocking voltage of the heavily degraded module of 800 V in Fig. 4 (right). The small changes in the determined breakdown voltage in Fig. 4 (left) and (right) might be caused by differences in the ambient temperature, since changes in room temperature cannot be excluded between the measurements. However, the results show that the degradation of the high-side switch and even the severeness of the degradation are detected successfully.

## Conclusion

This paper presents a first approach to the practical implementation of a concept for the in-situ detection of humidity-related degradation of IGBT modules in a full-scale, back-to-back converter usually used in wind turbines, which was previously tested only on a laboratory scale in [7].

The measured current  $I_M$  reveals that the leakage current is dominated by an additional resistance, which is identified as the resistance of the collector-sense circuit attached to the gate driver. The influence of this external resistance could be calculated and subtracted from the measured data in order to determine the leakage current through the switches. However, other influences such as temperature, tolerances, etc., on the resistance must be taken into account. A substantial increase in the leakage current is detectable, but might still meet the specifications given on the module datasheet. The results also show that not only the modules but also the gate driver is monitored. Therefore, a change in the  $I_M$ - $V_M$  characteristic cannot be clearly assigned to the gate driver, the module or other components. Nevertheless, this would suggest a notable change in the system compared to the original state, which would indicate some kind of degradation or damage to the system. Ultimately, the entire system must be observed from the beginning or characterised in advance in order to obtain a lookup table for the initial system under different environmental conditions, such as temperatures. Only then can a statement about the degradation of the system be made.

To exploit the concept to the fullest extent, the applied DC-link voltage  $V_{dc}$  during the measurement should be higher than the nominal DC-link voltage during operation  $V_{dc,N}$ . The DC-link voltage in an active blocking state of both converters (LSC and MSC) can be set by the additional precharge circuit. Since the voltage supplied by the precharge circuit is normally chosen to be below the nominal DC-link voltage  $V_{dc,N}$ , only modules which exhibit an increase in leakage current as the result of humidity-related degradation could be monitored in this case. Otherwise, the precharge circuit needs to be adjusted to provide a higher DC-link voltage  $V_{dc}$ . This would enable modules which show a reduction in the breakdown voltage to be monitored as well.

In this work, the precharge circuit has been adjusted so that the DC link could be charged up to 1200 V. To avoid the chopper turning on, it was deactivated for the time of the measurement. This work shows that it is possible to conduct the measurement safely inside the full-scale, back-to-back converter during the standstill phases of wind turbines, even though the DC-link voltage  $V_{dc}$  is above the nominal DC-link voltage  $V_{dc,N}$ . Moreover, it has been shown that the detection of humidity-related degradation is possible and even its severeness may be distinguished.

## References

- [1] K. Fischer, M. Steffes, K. Pelka, B. Tegtmeier, and M. Dörenkämper, “Humidity in power converters of wind turbines—field conditions and their relation with failures,” *Energies*, vol. 14, no. 7, p. 1919, 2021.
- [2] K. Fischer, K. Pelka, A. Bartschat, B. Tegtmeier, D. Coronado, C. Broer, and J. Wenske, “Reliability of power converters in wind turbines: Exploratory analysis of failure and operating data from a worldwide turbine fleet,” *IEEE Transactions on Power Electronics*, vol. 34, no. 7, pp. 6332–6344, 2019.
- [3] C. Zorn and N. Kaminski, “Acceleration of temperature humidity bias (thb) testing on igbt modules by high bias levels,” in *2015 IEEE 27th International Symposium on Power Semiconductor Devices & IC's (ISPSD)*. IEEE, 10.05.2015 - 14.05.2015, pp. 385–388.
- [4] D. Herwig, T. Brockhage, and A. Mertens, “Combining multiple temperature-sensitive electrical parameters using artificial neural networks,” in *2020 22nd European Conference on Power Electronics and Applications (EPE'20 ECCE Europe)*, 2020, pp. 1–10.
- [5] M. A. Eleffendi and C. M. Johnson, “In-service diagnostics for wire-bond lift-off and solder fatigue of power semiconductor packages,” *IEEE Transactions on Power Electronics*, vol. 32, no. 9, pp. 7187–7198, 2017.
- [6] W. Holzke, A. Brunko, H. Groke, N. Kaminski, and B. Orlik, “A condition monitoring system for power semiconductors in wind energy plants,” in *PCIM Europe 2018; International Exhibition and Conference for Power Electronics, Intelligent Motion, Renewable Energy and Energy Management*, 2018, pp. 1–7.
- [7] B. Kostka, D. Herwig, M. Hanf, C. Zorn, and A. Mertens, “A concept for detection of humidity-driven degradation of igbt modules,” *IEEE Transactions on Power Electronics*, vol. 36, no. 12, pp. 13 355–13 359, 2021.
- [8] K. Fischer, T. Stalin, H. Ramberg, J. Wenske, G. Wetter, R. Karlsson, and T. Thiringer, “Field-experience based root-cause analysis of power-converter failure in wind turbines,” *IEEE Transactions on Power Electronics*, vol. 30, no. 5, pp. 2481–2492, 2015.